JOURNAL OF DECISION MAKING AND HEALTHCARE
Volume 1 (2024), No. 1, 1–15
https://doi.org/10.69829/jdmh-024-0101-ta01
Tulipa Opera Scholarum

A DATA PRE-PROCESSING WITH MASS-PRESERVING OPTIMAL MASS TRANSPORTATION FOR BRAIN TUMOR SEGMENTATION

TSUNG-MING HUANG[1], JIA-WEI LIAO[2], WEN-WEI LIN[3], AND HAO-REN YAO[4,*]

[1] *Department of Mathematics, National Taiwan Normal University, Taipei 116, Taiwan*
[2] *Department of Computer Science and Information Engineering, National Taiwan University, Taipei 106, Taiwan*
[3] *Department of Applied Mathematics, National Yang Ming Chiao Tung University, Hsinchu 300, Taiwan*
[4] *National Institutes of Health, Bethesda, MD, USA*

Abstract. This article aims to build a framework of brain tumor segmentation for 3D MRI brain images by using the UNet-based deep learning method with optimal mass transportation (OMT) for data pre-processing. For this purpose, we develop a novel 2-phase UNet-based OMT to increase the ratio of brain tumors in the input OMT tensors. Moreover, due to the scarcity of training data, we change the density function by different parameters to increase the data diversity. For the post-processing, we propose an adaptive ensemble procedure by computing the eigenvector of the Dice similarity matrix corresponding to the largest eigenvalue and then using it to aggregate the probability as the predicted label. Using SegResUNet with OMT input tensors to train the data for the adult glioma (Task 1), Sub-Sahara-Africa adult glioma (Task 2), and meningioma (Task 3) in the international Brain Tumor Segmentation Cluster of Challenges 2023, the Dice scores of (whole tumor, tumor core, enhanced tumor) for online validations of Tasks 1, 2, and 3 are (0.9214, 0.8823, 0.8411), (0.8747, 0.8344, 0.8267), and (0.8316, 0.8395, 0.8401), respectively. Compared with random crop pre-processing, OMT is far superior.

Keywords. Optimal Mass Transportation, Density function, 2-Phase UNet-based OMT, Brain Tumor Segmentation.

1. Introduction

Gliomas are the most common type of malignant adult brain tumors. WHO divides glioblastoma into grades 1 to 4. The higher the grade, the more malignant it is. Glioblastoma, a WHO grade 4 astrocytoma, is extremely intrinsically heterogeneous in appearance, shape, and histology. Isocitrate dehydrogenase (IDH) mutation status has been suggested as the most critical marker for glioma diagnostic decisions [21]. IDH mutation status on magnetic resonance imaging (MRI) can be accurately and objectively predicted using deep learning [6, 8, 24]. Most deep-learning studies need to automatically segment glioma regions along the edge of the lesion [9]. Therefore, brain tumor detection and segmentation from MRI are essential tasks.

Brain tumors, in general, are challenging to diagnose from MRI scans. The Brain Tumor Segmentation (BraTS) Challenge dataset [1, 4, 2, 3, 19] has provided a formidable platform. It has been designed to encourage research in medical image segmentation to develop deep-learning algorithms that can accurately segment brain tumors from MRI scans. BraTS Cluster of Challenges 2023 contains about 4500 benchmark 3D MRI brain images with nine tasks, of which five tasks are the brain tumor segmentation of whole tumor (WT), tumor core (TC), and enhanced tumor (ET) regions in the human brain. Tasks 1-5 are the segmentations of the adult glioma, Sub-Sahara-Africa adult glioma, meningioma, brain metastases, and pediatric tumors, respectively. Each MRI brain image contains four modalities, namely,

*Corresponding author.
E-mail address: hy301@georgetown.edu (H.-R. Yao)
Accepted: February 28, 2024.

native (T1), post-contrast T1-weighted (T1Gd), T2-weighted (T2), and T2 Fluid Attenuated Inversion Recovery (T2-FLAIR). Each modality is a $240 \times 240 \times 155$ tensor image.

In the past decade, U-Net-based neural networks have become an essential and effective method for medical image segmentation. In particular, remarkable achievements have been achieved in brain tumor segmentation. The encoder-decoder architecture with skip connections, introduced in the U-Net [7, 22], has outperformed other traditional methods in brain glioma segmentation [13, 17]. These works focus on the developed deep-learning algorithms for targeting brain tumor segmentation. Recently, an ensemble of DeepSeg [30], nnU-Net [13], and DeepSCAN [18] for automatic glioma boundaries detection in pre-operative MRI is proposed in [29]. There are few discussions about the pre-processing of the data.

Random cropping of the raw brain images is often used as the data pre-processing in deep learning for brain tumor segmentation. However, it needs more croppings to cover entire regions of the brain image [22]. To adequately address the 3D structure, a two-stage mass-preserving optimal mass transport (OMT) is proposed to transform an irregular 3D MRI brain image into a $128 \times 128 \times 128$ cube [14, 15]. The OMT map satisfies the minimal deformation on the set of volume- or mass-preserving mappings and preserves the global information of the brain image.

The main task of this paper is focused on using our proposed mass-preserving OMT map to deal with the data pre-processing in brain tumor segmentation. We are using these OMT tensors as deep learning input to segment brain tumors accurately for medical brain images. Specifically, we transform the irregular 3D parenchymal brain image into a $128 \times 128 \times 128$ OMT tensor and use the characteristics of OMT to design the appropriate density function to enlarge the possible tumor region in the OMT tensor. Furthermore, we can conveniently augment data by distributing different density function parameters to increase data diversity, effectively performing accurate segmentation for brain tumors.

The main contributions of this paper are twofold.

(i) By controlling the density of the possible tumor region and its surroundings, the OMT map between the brain image and the 128^3 cube can properly enlarge the tumor region in the cube, which is very beneficial for deep learning in identifying and predicting labels. We propose two-phase U-Net-based OMT deep learning to predict and segment the tumor region. The goal of Phase I is used to indicate the possible tumor region. Phase II is a data pre-processing and segmentation of the brain tumor, which transforms the brain image into an OMT tensor with the density function defined by the predicted tumor region. Furthermore, we can make effective data augmentation through different density control to increase the robustness of the model.

For the post-processing, we propose an adaptive ensemble procedure by computing the eigenvector, a probability distribution, of the Dice similarity matrix corresponding to the largest eigenvalue and then using this eigenvector to aggregate the ensembling probabilities as the predicted label.

(ii) To demonstrate the effect of our proposed data pre-processing and adaptive ensemble, we use Residual UNet [25], SegResNet [20], SwinUNETR [10], HarDNet-FCN [5, 16] as our benchmark training models to predict and segment the tumor regions for Tasks 1-3 in BraTS 2023 dataset. The Dice scores in Tables 3 and 4 show that these data pre-processing techniques suit these training models and get reasonable Dice scores for Task 1. Using SegResUNet with OMT input tensors, the Dice scores of (WT, TC, ET) for online validations of Tasks 1, 2, and 3 are (0.9214, 0.8823, 0.8411), (0.8747, 0.8344, 0.8267), and (0.8316, 0.8395, 0.8401), respectively, which demonstrates our proposed method can be applied to detect and segment the brain tumor for different dataset.

This paper is organized as follows. In Section 2, we introduce the data pre-processing by the area-measure-preserving and volume-measure-preserving OMT maps. Then, we propose a two-phase UNet-based deep learning method and an adaptive ensemble to predict the tumor region. In Section 3, we

introduce the setup of the training method. Numerical results are introduced in Section 4. Finally, concluding remarks are given in Section 5.

2. Methods

2.1. **Two-Stage OMT Map.** To preserve the global information of the 3D MRI brain image, the optimal mass transportation (OMT) with mass-preserving parameterizations [14, 15, 26] is proposed to transform the irregular brain image into a solid unit ball $\mathcal{B}^3$, which minimizes the transport cost and preserves the local mass ratios. Let $\mathcal{M}$ be a simplicial 3-complex that describes an irregular 3D brain image with a genus-zero boundary, where $\mathcal{M}$ is a tetrahedral mesh composed of sets of vertices $\mathbb{V}(\mathcal{M})$, edges $\mathbb{E}(\mathcal{M})$, faces $\mathbb{F}(\mathcal{M})$ and tetrahedrons $\mathbb{T}(\mathcal{M})$.

Let ρ be a density map on $\mathbb{V}(\mathcal{M})$. Denote

$$\mathbf{G}_\rho = \left\{ g : \partial\mathcal{M} \to \partial\mathcal{B}^3 \;\middle|\; \rho(\alpha)|\alpha| = |g(\alpha)|,\ \forall \alpha \in \mathbb{F}(\partial\mathcal{M}) \right\}$$

and

$$\mathbf{F}_\rho = \left\{ f : \mathcal{M} \to \mathcal{B}^3 \;\middle|\; \rho(\tau)|\tau| = |f(\tau)|,\ \forall \tau \in \mathbb{T}(\mathcal{M}) \right\}$$

as the sets of all area-measure-/mass-preserving piecewise linear maps, where $|\alpha|$ and $|\tau|$ are the area and volume of α and τ, respectively. The spherical area-preserving parameterization $g \in \mathbf{G}_\rho$ with $g(\widehat{\mathbf{v}}_i) = (g_i^1, g_i^2, g_i^3)$, $i = 1, \ldots, m \equiv \#\mathbb{V}(\partial\mathcal{M})$, $\mathbf{g}^t = (g_1^t, \ldots, g_m^t)^\top$, $t = 1, 2, 3$ and $\mathbf{g} = [\mathbf{g}^1, \mathbf{g}^2, \mathbf{g}^3] \in \mathbb{R}^{m\times 3}$ can be computed by minimizing stretch energy [28] defined as

$$E_S(g) = \tfrac{1}{2}\text{trace}\left(\mathbf{g}^* L_S(g)\mathbf{g}\right),$$

in which $L_S(g)$ is the stretched Laplacian matrix defined as

$$[L_S(g)]_{i,j} = \begin{cases} -\frac{1}{2}\left(\frac{\cot(\theta_{i,j}(g))}{\sigma_{g^{-1}}([v_i,v_j,v_k])} + \frac{\cot(\theta_{j,i}(g))}{\sigma_{g^{-1}}([v_j,v_i,v_\ell])}\right) & \text{if } [v_i, v_j] \in \mathbb{E}(\mathcal{M}), \\ -\sum_{\ell\neq i}[L_S(g)]_{i,\ell} & \text{if } j = i, \\ 0 & \text{otherwise,} \end{cases}$$

where $\sigma_{g^{-1}} : \mathbb{F}(\mathcal{M}) \to \mathbb{R}$ is the local stretch factor defined as

$$\sigma_{g^{-1}}(\alpha) := \frac{\rho(\alpha)|\alpha|}{|g(\alpha)|}, \quad \alpha \in \mathbb{F}(\partial\mathcal{M}),$$

$\theta_{i,j}(g)$ and $\theta_{j,i}(g)$ are two angles opposite to edge $g([v_i, v_j])$. A stretch energy minimization (SEM) algorithm is proposed in [28] to compute the minimizer of $E_S(g)$. Furthermore, the volumetric stretch energy minimization (VSEM) algorithm [27] with fixed a given spherical area-preserving parameterization $\hat{g} \in \mathbf{G}_\rho$ as the boundary sphere of $f \in \mathbf{F}_\rho$ is proposed to compute the mass-preserving parameterization f by minimizing the volume-weighted stretch energy [27] defined as

$$E_V(f) = \frac{1}{2}\text{trace}\left(\mathbf{f}^\top L_V(f)\,\mathbf{f}\right), \tag{2.1}$$

where $L_V(f)$ is the mass-weighted Laplacian matrix with

$$[L_V(f)]_{i,j} = \begin{cases} -w_{i,j}(f) & \text{if } [v_i, v_j] \in \mathbb{E}(\mathcal{M}), \\ \sum_{\ell\neq i} w_{i,\ell}(f) & \text{if } j = i, \\ 0 & \text{otherwise,} \end{cases}$$

in which $w_{i,j}(f)$ is the stretched cotangent weight given by

$$w_{i,j}(f) = -\frac{1}{9}\sum_{k,\ell} \frac{|f([\mathbf{v}_i, \mathbf{v}_k, \mathbf{v}_\ell])||f([\mathbf{v}_j, \mathbf{v}_\ell, \mathbf{v}_k])| \cos\theta_{i,j}^{k,\ell}(f)}{\rho(\tau)|\tau|}$$

with the dihedral angle $\theta_{i,j}^{k,\ell}(f)$ between $[\mathbf{f}_i, \mathbf{f}_k, \mathbf{f}_\ell]$ and $[\mathbf{f}_j, \mathbf{f}_\ell, \mathbf{f}_k]$. Here, $\mathbf{f}_t = f(\mathbf{v}_t) = (f_t^1, f_t^2, f_t^3) \in \mathbb{R}^3$, for $t = 1, \ldots, n \equiv \#\mathbb{V}(\mathcal{M})$ and $\mathbf{f} = [\mathbf{f}_1^\top, \cdots, \mathbf{f}_n^\top]^\top \in \mathbb{R}^{n\times 3}$. The R-linear convergence of SEM and VSEM have been proved in [12] and [11], respectively.

The discrete OMT problems on $\partial\mathcal{M}$ and $\mathcal{M}$ with respect to $\|\cdot\|_2$ consist of finding a $g_\rho^* \in \mathbf{G}_\rho$ and $f_\rho^* \in \mathbf{F}_\rho$ that solve optimal problems

$$g_\rho^* = \underset{g\in\mathbf{G}_\rho}{\operatorname{argmin}} \sum_{\hat{\mathbf{v}}\in\mathbb{V}(\partial\mathcal{M})} \|\hat{\mathbf{v}} - g(\hat{\mathbf{v}})\|_2^2 a_\rho(\hat{\mathbf{v}}) \equiv \underset{g\in\mathbf{G}_\rho}{\operatorname{argmin}} \mathcal{C}_0(g), \tag{2.2a}$$

$$f_\rho^* = \underset{f\in\mathbf{F}_\rho}{\operatorname{argmin}} \sum_{\mathbf{v}\in\mathbb{V}(\mathcal{M})} \|\mathbf{v} - f(\mathbf{v})\|_2^2 m_\rho(\mathbf{v}) \equiv \underset{f\in\mathbf{F}_\rho}{\operatorname{argmin}} \mathcal{C}(f), \tag{2.2b}$$

where $a_\rho(\hat{\mathbf{v}})$ and $m_\rho(\mathbf{v})$ are the local area/volume measures at $\hat{\mathbf{v}} \in \mathbb{V}(\partial\mathcal{M})$ and $\mathbf{v} \in \mathbb{V}(\mathcal{M})$, respectively, defined as

$$a_\rho(\hat{\mathbf{v}}) = \frac{1}{3} \sum_{\alpha\in N(\hat{\mathbf{v}})} \rho(\alpha)|\alpha|, \quad m_\rho(\mathbf{v}) = \frac{1}{4} \sum_{\tau\in N(\mathbf{v})} \rho(\tau)|\tau|,$$

in which $N(\mathbf{v})$ is the set of 1-ring neighboring tetrahedrons of $\mathbf{v}$. A projected gradient method with using SEM algorithm as a projector is proposed in [26] to compute the area-measure-preserving OMT map g_ρ^* in (2.2a). Using VSEM algorithm with fixed this unit sphere g_ρ^* as a projector, a projected gradient method, called V-OMT algorithm, is proposed in [11] to compute f_ρ^* in (2.2b).

Now, we can apply the V-OMT algorithm to transform an irregular 3D brain image $\mathcal{M}$ into a cube $\mathcal{C}$ to satisfy the input format of the 3D Unet-based deep learning. To compute the cubic mass-preserving OMT map $\hat{f}_\rho^*$ from $\mathcal{M}$ to $\mathcal{C}$, we utilize the V-OMT algorithm to compute the mass-preserving OMT maps $f_\rho^* : \mathcal{M} \to \mathcal{B}^3$ and $f_1^* : \mathcal{C} \to \mathcal{B}^3$ ($\rho = 1$), respectively. Then, the composition map $\hat{f}_\rho^* = (f_1^*)^{-1} \circ f_\rho^* : \mathcal{M} \to \mathcal{C}$, as shown in Figure 1, is the desired cubic mass-preserving OMT map.

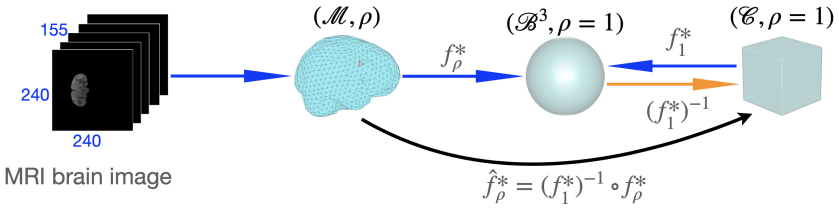

FIGURE 1. A diagram illustrating the construction of the OMT map $\hat{f}_\rho^*$ between $(\mathcal{M}, \rho)$ and $(\mathcal{C}, \rho \equiv 1)$

2.2. **Two-Phase UNet-based OMT for training and testing sets.** From the definition of mass-preserving map, i.e., $\rho(\tau)|\tau| = |f(\tau)|$, the tumor region in cube $\mathcal{C}$ will be enlarged if the density of the tumor in the brain image $\mathcal{M}$ is larger than 1. This will be helped to detect and segment the tumor region in the deep learning. In general, as shown in Figure 2, the FLAIR modality of the adult glioma typically reflects the distribution of WT and the grayscale values of the WT region are greater than those of other regions. Therefore, the adapted grayscales on the voxel can help with defining the density map on $\mathbb{V}(\mathcal{M})$. Let $\mathbb{H}_\mathbf{e}$ denote the normalized contrast-enhanced histogram equalization grayscale values of the FLAIR modality of a brain image and $\mathbb{H}_\mathbf{e}(v)$ denote the value of $\mathbb{H}_\mathbf{e}$ at the voxel v. According to $\mathbb{H}_\mathbf{e}$, the associated density function ρ_γ on the voxel v belonging to the brain is defined as

$$\rho_\gamma(v) = \exp(\gamma \mathbb{H}_\mathbf{e}(v)), \tag{2.3}$$

where γ is a hyper-parameter chosen from the interval $[0, 2]$. However, density function ρ_γ in (2.3) not only enlarge the tumor region but also enlarge the other region. To tackle this problem, we define a step-like density function

$$\rho_\gamma^s(v) = \begin{cases} \exp(\gamma \mathbb{H}_{\mathbf{e}}(v)), & \text{if } v \in \text{WT region}, \\ 1, & \text{otherwise}. \end{cases} \tag{2.4}$$

and construct a new smooth density function $\hat{\rho}_\gamma$ using the image filtering technique by convolving ρ_γ^s in (2.4) with a $m \times m \times m$ blur box tensor, as follows:

$$\hat{\rho}_\gamma(v) = \rho_\gamma^s(v) \otimes \frac{\mathbb{1}_{m\times m\times m}}{m^3}, \quad v \in \mathcal{M}. \tag{2.5}$$

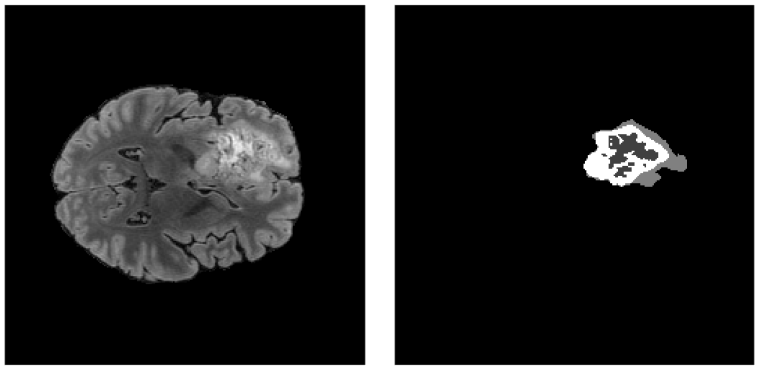

(A) brain (B) tumor

FIGURE 2. Brain image of FLAIR modality for the adult glioma and the associated tumor region

For the 3D brain images in the training set, we can apply the two-stage OMT method with the density function $\hat{\rho}_\gamma$ in (2.5) and the given WT label region to transform the brain image with four modalities into a $128 \times 128 \times 128 \times 4$ tensor. But we can not directly apply $\hat{\rho}_\gamma$ to construct the OMT map for the validation and testing data because we need to estimate the associated WT region firstly. A novel 2-Phase UNet-based algorithm combined with optimal mass transport (2P-UNetB-OMT) for the training and inference has been proposed in [15] as shown in Figure 3. In Phase I, the density function ρ_γ in (2.3) is applied to construct the $128 \times 128 \times 128 \times 4$ OMT tensors. The UNet-based model with these input tensors is used to train a model to accurately detect the possible WT region of the validation and testing data. In Phase II, the possible tumor regions of WT are expanded by m voxels with morphology dilation, denoted by $\mathcal{R}_w \subseteq \mathcal{M}$, and modify ρ_γ^s in (2.4) for the validation and testing data as

$$\rho_\gamma^s(v) = \begin{cases} \exp(\gamma \mathbb{H}_{\mathbf{e}}(v)), & \text{if } v \in \mathcal{R}_w, \\ 1, & \text{otherwise}. \end{cases} \tag{2.6}$$

The new $128 \times 128 \times 128 \times 4$ OMT tensors for the training data and validation/testing data are then constructed by using density $\hat{\rho}_\gamma$ in (2.5) with ρ_γ^s in (2.4) and (2.6), respectively. The UNet-based model with new OMT tensors is applied to train a new model to predict the WT, TC, and ET of the validation/testing data.

By defining the density function, we want to enlarge the tumor region after the OMT map. But, when the grayscale values of the tumor region do not larger than those of other brain region as shown in Figure 4, the percentage of the tumor region in OMT tensor may be less than that in raw brain region. For example, for the MRI 3D brain image in Figure 4, the percentages of the tumor region in raw 3D

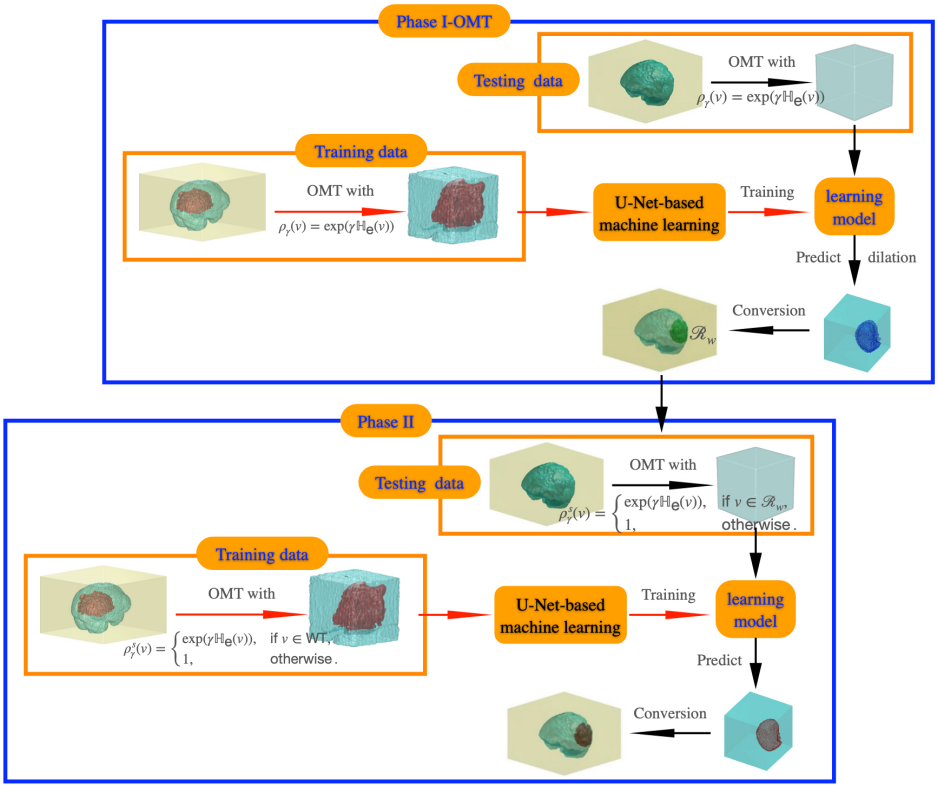

FIGURE 3. A flow chart of 2P-UNetB-OMT framework

brain region and OMT tensor region for Phase I with $\gamma = 1$ are 0.00963 and 0.00878, respectively. The tumor region in OMT tensor is minified. Since Phase I is just used to detect the possible WT region of the validation/testing data, we can use UNet-based model, e.g., Residual UNet and SegResNet, with raw brain images to train a model and then predict the possible WT region. In this paper, we use UNet-based model with random crop pre-processing for the raw brain images to replace the mass-preserving OMT tensors in Phase I, which is shown in Figure 5, and call the algorithm of Phase II with random crop Phase I as 2P-Crop-OMT-UNetB algorithm.

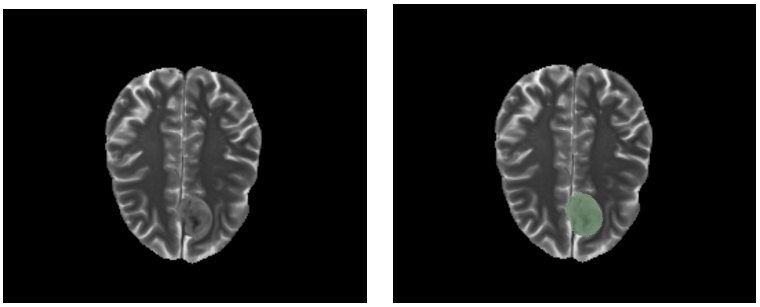

(A) brain (B) tumor (green region)

FIGURE 4. Brain image of T2 modality for the meningioma and the associated tumor region

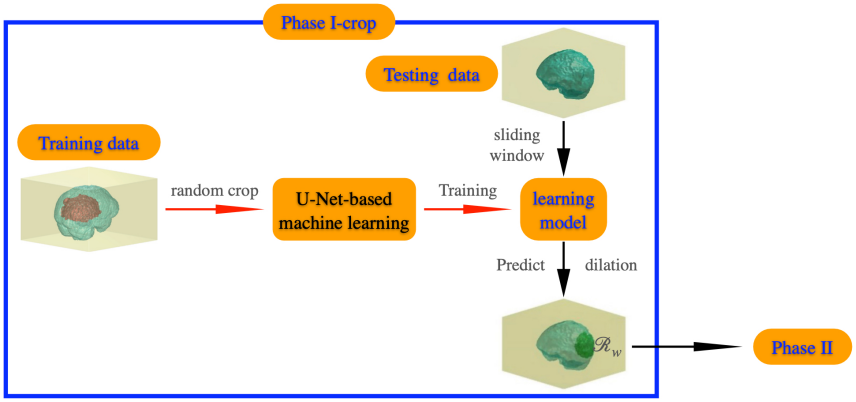

FIGURE 5. A flow chart of Phase I with random crop pre-processing for the raw brain images

2.3. **Data Augmentation.** The OMT with mass-preserving parameterizations transform the irregular brain image into a solid unit ball $\mathcal{B}^3$ to preserve the global information of the 3D MRI brain image. Furthermore, the tumor region in the OMT tensor can be enlarged by the various hyper-parameter γ in (2.4) and (2.6). This means that for a 3D MRI brain image we can construct many OMT tensors with different tumor regions by using various hyper-parameter γ. Each OMT tensor keeps the global information of the brain image so that we can use them to augment the training tensors to increase data diversity. Here, we take $\gamma = 1.0$, 1.5, 1.75, and 2.0 in (2.4) for n training brain samples to obtain $4n$ augmented training OMT tensors.

To avoid over-fitting and enhance the robustness of a model, we can apply the data augmentation techniques to these $4n$ tensors and from which we choose n tensors to train the model. In this paper, we use following data augmentation techniques:

: (Au1). **Randomly flipping:** With probability 0.25, we flip the image left and right.
: (Au2). **Randomly rotating:** With probability 0.25, we rotate the image counterclockwise by 90 degrees.
: (Au3). **Randomly adjusting brightness:** With probability 0.1, we set the bright value range from 0.9 to 1.1 and modify the grayscale. Then we truncate the bright value to [0, 1] if necessary.
: (Au4). **Randomly adding noise:** With probability 0.1, we add the Gaussian noise with a standard deviation of 0.01 to the grayscale image.
: (Au5). **Normalized image:** We rescale the grayscale range to [0, 1] using Min-Max normalization.

2.4. **The Adaptive Ensemble Method.** In this subsection, we propose a novel ensemble method for the validation and testing sets that can adapt the weight of aggregation by solving the eigenvector of the Dice similarity matrix.

According to the expanded WT region of the validation (testing) set in Phase I, the irregular 3D brain samples are transformed into $128\times128\times128\times4$ OMT tensors with density functions ρ^s_γ and $\hat{\rho}_\gamma$ in (2.6) and (2.5), respectively. Here, we take $\gamma = 1.5$. For each OMT tensor (called $\mathcal{R}_1$), we further construct $(m-1)$ $128\times128\times128\times4$ tensors (called $\mathcal{R}_2, \ldots, \mathcal{R}_m$) by using data augmentation techniques to $\mathcal{R}_1$, e.g. flipping, rotating, noise in Section 2.3. Therefore, we have m tensors for each brain image sample. In the training process, we choose ℓ training models at k_1-th, ..., k_ℓ-th epoch. Let $P_{i+(j-1)m}$ denote the probability of the prediction $\mathcal{L}_{i+(j-1)m}$ of the brain image from the tensor $\mathcal{R}_i$ by using the training model j for $i = 1, \ldots, m$, $j = 1, \ldots, \ell$. Our goal is to aggregate $\{P_i \mid i = 1, \ldots, m\ell\}$ to get the finial

prediction. In what follows, we propose a method that automatically detects outliers and gives a higher weight to the important prediction.

First, we compute the Dice similarity coefficient of $\{\mathcal{L}_i \mid i = 1, \ldots, m\ell\}$ pairwise, that is, $Dice(\mathcal{L}_i, \mathcal{L}_j)$ for $i, j = 1, \ldots, m\ell$, and form the matrix $D \equiv [Dice(\mathcal{L}_i, \mathcal{L}_j)]$ as shown in Figure 6. Let $\mathbf{v} = (v_1, \cdots, v_{m\ell})^\top$ with $\|\mathbf{v}\|_1 = 1$ be the eigenvector of D corresponding to the largest eigenvalue $\lambda_{\max}$. Since $D \geq 0$ is irreducible, by Perron-Frobenius Theorem, $\lambda_{\max} = \rho(D)$ and $0 < v_i < 1$ for $i = 1, \ldots, m\ell$. That is $\mathbf{v}$ is a probability distribution. Then we define the final probability $\widehat{P}$ as

$$\widehat{P} = \sum_{i=1}^{m\ell} v_i P_i.$$

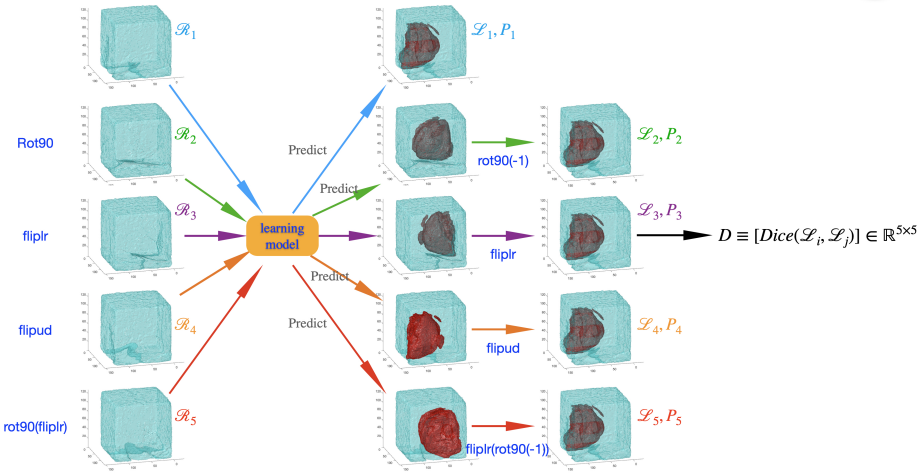

FIGURE 6. Adaptive Ensemble Processing: Assume there are five predictions $\{\mathcal{L}_1, \ldots, \mathcal{L}_5\}$ with probabilities $\{P_1, \ldots, P_5\}$ of the brain image. Let $D = [Dice(\mathcal{L}_i, \mathcal{L}_j)] \in \mathbb{R}^{5\times5}$ and $\mathbf{v} = [v_i]$ with $\|\mathbf{v}\|_1 = 1$ be the eigenvector of D corresponding to the spectral radius $\rho(D)$. The ensembling probability $\widehat{P}$ is taken as $\widehat{P} = \sum_{i=1}^{5} v_i P_i$.

3. TRAINING SETUP

3.1. **Model Architecture.** To predict the regions of WT, TC, and ET at the same time in Phase II, we develop a multi-head mechanism, which contains three decoders at the end of the model, in the UNet-based training model as shown in Figure 7. Since tumors have an inclusion relation ET $\subseteq$ TC $\subseteq$ WT, we add the output of the ET decoder to the output of the TC decoder and the output of the TC decoder to the output of the WT decoder. The multi-head mechanism can be applied to Residual UNet, SegResNet, SwinUNETR, and HarDNet-FCN, which are the common UNet-based models.

3.2. **Loss Function.** The segmentation task can be seen as pixel-wise classification. The most popular loss function in classification tasks is cross-entropy. However, if the cross-entropy is chosen for the segmentation task, it will suffer from a foreground and background imbalance problem; that is, the loss is small when the objective region is small. To deal with this issue, we adopt the combination of dice loss

$$\mathcal{L}_{Dice}(P, G) = 1 - \frac{2\sum_{i,j,k,c} P_{i,j,k,c} G_{i,j,k,c}}{\sum_{i,j,k,c} P_{i,j,k,c} + \sum_{i,j,k,c} G_{i,j,k,c}}$$

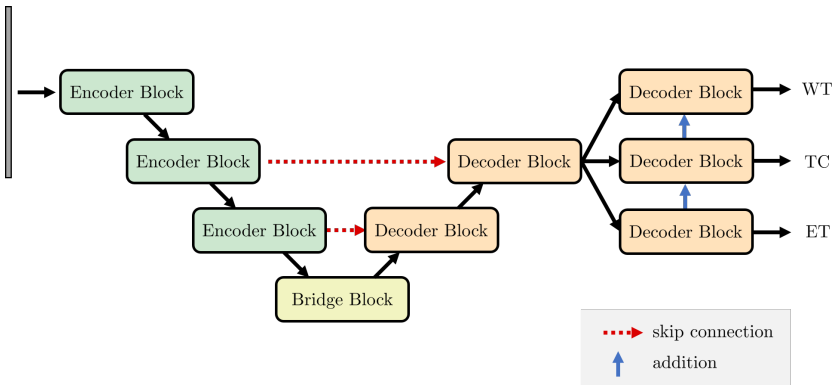

FIGURE 7. Architecture of the multi-head mechanism

and focal loss

$$\mathcal{L}_{FL}(P,G) = -\sum_{i,j,k} \alpha\,(1-P_{i,j,k,C})^{\gamma}\log P_{i,j,k,C},$$

where C is the category of $G_{i,j,k}$ and $\alpha, \gamma \geq 0$ are hyperparameters, as the segmentation loss, in which $P, G \in \mathbb{R}^{n\times m\times p\times q}$ are the prediction and ground truth, respectively.

3.3. **Learning rate.** It is known that the deep learning model is very sensitive to the initial weights. If we choose a high learning rate, it may bring instability to the resulting model. The warm-up method is used to guarantee the gradual stabilization of the model at the beginning. Let γ_{max} and γ_{min} be the maximum and minimum learning rates, respectively, i_{warm} be the warm up iteration, and i_t be the total iteration. Then, we adopt the learning rate γ_i with the cosine decay and warm-up mechanism at the i-th iteration as

$$\gamma_i = \begin{cases} \frac{\gamma_{max}}{i_{warm}} i, & \text{if } i \leq i_{warm} \\ \gamma_{min} + \frac{1}{2}(\gamma_{max}-\gamma_{min})\left(1+\cos\left(\frac{i-i_{warm}}{it-i_{warm}}\pi\right)\right), & \text{if } i > i_{warm}. \end{cases}$$

4. RESULTS

Brain Tumor Segmentation (BraTS) 2023 Cluster of Challenges contains 9 tasks. In this section, we focus on Tasks 1, 2, and 3. Task 1 is the same adult glioma population as in the RSNA-ANSR-MICCAI BraTS 2021 Continuous Challenge [1, 4, 2, 3, 19]. Tasks 2 and 3 are the underserved sub-Saharan African brain glioma patient population and intracranial meningioma, respectively.

: (i). BraTS 2021 Continuous Challenge database contains 2,040 brain images with 1,251 training images and 219 unlabeled brain image samples for validation. The others are unreleased brain image samples for testing. For the 1,251 brain image samples, we randomly choose 1,000 samples for training and 251 for cross-validation.

: (ii). The Sub-Sahara-Africa Adult Glioma contains 60 training images, randomly chosen 48 samples for training and 12 for cross-validation, and 15 unlabeled brain image samples for online validation.

: (iii). ASNR-MICCAI BraTS Intracranial Meningioma Challenge contain 1,000 training MRI images, randomly chosen 800 samples for training and 200 for cross-validation, and 141 unlabeled brain image samples for online validation.

Residual UNet, SegResNet, SwinUNETR, and HarDNet-FCN are the common UNet-based models. In this section, we compare the predicted results of the cross and online validations for using these UNet-based models to demonstrate the accuracy of the brain tumor segmentation by using the proposed

preprocessing and post processing techniques. Here, Residual UNet, SegResNet, and SwinUNETR are implemented in PyTorch and the Medical Open Network for AI (MONAI) [23], and HarDNet-FCN is downloaded from the open source GitHub. The parameters of experiment models are shown in Table 1 with the batch size being 12 and the total epochs being 1,000. All trainings are performed on a linux server equipped with two NVIDIA Tesla A100 PCIe 40 GB GPUs.

TABLE 1. Parameters of the experiment models

Model	Initial Filters	Width	Depth	Activation	Norm	Dropout
Residual UNet	32	2	4	PReLU	Instance	0.25
HarDNet-FCN	32	1	4	Mish	Instance	0.1
SegResNet	32	2	3	ReLU	Instance	0.25
SwinUNETR	32	1	4	LeakyReLU	Instance	0

In Phase II, we compute OMT maps with the smooth density functions $\hat{\rho}_\gamma$ with $\gamma = 1.0, 1.5, 1.75,$ and 2.0 in (2.5) with ρ^s_γ in (2.4) for 1,000 brain samples to obtain 4,000 augmented $128 \times 128 \times 128 \times 4$ OMT tensors. The techniques (Au1)-(Au5) in Section 2.3 are used to randomly generate 1,000 training samples from 4,000 augmented OMT tensors. Furthermore, for cross-validation and online validation, the density function $\hat{\rho}_\gamma$ with ρ^s_γ in (2.6) and $\mathcal{R}_w$ in Phase I are used to compute the associated $128 \times 128 \times 128 \times 4$ OMT tensors.

For the adaptive ensemble in Section 2.4 of the cross-validation and online validation, we select the three learning models $(\ell = 3)$ at epoch k_1, k_2, k_3, which have the first three best Dice scores, and use the techniques (Au1)-(Au5) $(m = 6)$ to augment the validation OMT tensors in each epoch. That is we aggregate $m\ell = 18$ predictions to determine the finial prediction.

4.1. **2P-UNetB-OMT algorithm for BraTS 2021 Continuous Challenge.** In the first, we compare the Dice scores of 219 online validation samples in Phase I with $128 \times 128 \times 128 \times 4$ OMT tensors for Residual UNet, HarDNet-FCN and SegResNet. Here, we take $\gamma = 1.5$ in (2.3) to construct the density function. The WT dice scores for online validation are 0.9154, 0.9174, and 0.9204 for Residual UNet, HarDNet-FCN and SegResNet, respectively. This result shows the learning model produced by SegResNet can get better Dice score than that Residual UNet and HarDNet-FCN. To compare Phase I-crop in Figure 5, we take twice random crop pre-processing, provided by MOANAI, for each raw brain image to obtain 2000 $128 \times 128 \times 128 \times 4$ training tensors. Table 2 shows the Dice scores of WT, TC, and ET of the online validation produced in Phase I-OMT and Phase I-crop. From Table 2, we can see that all Dice scores have improved by using OMT tensors in Phase I. Furthermore, SegResNet model can get more accuracy of the WT region for both Phase I-OMT and Phase I-crop. Therefore, we use such WT region to construct $\mathcal{R}_w$ in (2.6) for the validation samples in Phase II.

TABLE 2. Dice score of the online validation data for random crop and OMT

Model	Pre-processing	Online validation		
		WT	TC	ET
Residual UNet	Random Crop	0.9172	0.8586	0.8090
SegResNet	Random Crop	0.9194	0.8542	0.8242
SegResNet	OMT	0.9204	0.8683	0.8272

Similarly, we use Residual UNet, HarDNet-FCN, SwinUNETR as the training model in Phase II of 2P-UNetB-OMT algorithm and choose the three best models to perform the adaptive ensemble. The

associated final Dice scores of cross-validations and online validations for these four UNet-based models are shown in Table 3. These results show that the Dice score of WT produced by these three training models are only slightly different. There are obviously different for the Dice scores of TC and ET. From the results in Table 3, SegResNet produces the best Dice scores for WT, TC, and ET in these UNet-based training models. Compared the results of SegResNet in Table 3 with Table 2, the Dice scores of TC and ET have significantly improved in Phase II.

TABLE 3. Dice scores of WT, TC, and ET for cross-validation data and online validation data in 2P-UNetB-OMT algorithm with various UNet architectures

Model	Cross-validation			Online validation		
	WT	TC	ET	WT	TC	ET
Residual UNet	0.9307	0.9101	0.8602	0.9167	0.8560	0.8293
SegResNet	**0.9371**	**0.9152**	**0.8819**	**0.9214**	**0.8823**	**0.8411**
HarDNet-FCN	0.9349	0.9145	0.8554	0.9187	0.8676	0.7776
SwinUNETR	0.9330	0.9091	0.8686	0.9171	0.8568	0.8283

4.2. **2P-Crop-OMT-UNetB algorithm for BraTS 2021 Continuous Challenge.** In above, we discuss the Dice scores of WT, TC, and ET for using 2P-UNetB-OMT algorithm with four UNet-based models and find that SegResNet produces the best Dice scores. Therefore, we also use SegResNet as the training model of Phase II for 2P-Crop-OMT-UNetB algorithm. From Table 2, SegResNet in Phase I-Crop can get more accuracy of the WT region than that of Residual UNet. Thus, we use the WT region produced by SegResNet to construct $\mathcal{R}_w$ and take $\gamma = 1, 1.5, 1.75, 2$ to construct the OMT tensors for the validation samples.

For each γ, the learning models produced by Phase II with the adaptive ensemble is used to predict the associated validation OMT tensors. The predicted results of the Dice scores of WT, TC, and ET are shown in Table 4. In average, the Dice scores at $\gamma = 1.75$ is slightly better than that of the other three γ values. Comparing the result in Table 4 for $\gamma = 1.75$ with that of SegResNet in Table 3, we can see that the Dice scores produced by 2P-UNetB-OMT and 2P-Crop-OMT-UNetB are only slight different. They almost have the same prediction even they use different method in Phase I to detect the possible WT region. This indicates the importance of the OMT maps in Phase II. It is a stable method for brain tumor segmentation.

TABLE 4. Dice score of the 219 online validation produced by 2P-Crop-OMT-UNetB algorithm with various γ

γ	WT	TC	ET
$\gamma_1 = 1.0$	0.9227	0.8782	0.8398
$\gamma_2 = 1.5$	0.9208	0.8784	0.8455
$\gamma_3 = 1.75$	0.9228	0.8808	0.8420
$\gamma_4 = 2.0$	0.9221	0.8756	0.8424
$\gamma_1, \gamma_2, \gamma_3, \gamma_4$	0.9237	0.8815	0.8413

If the spending time for the inference is not an issue, then we can use multiple γ values to ensemble the final prediction. For example, we can use all above predictions (4×18) for $\gamma = 1, 1.5, 1.75, 2$ to get the final prediction. The last row of Table 4 shows the associated Dice score of WT, TC, and ET

for such 72 ensembles. The results show that the Dice scores of WT and TC have slight improvements. This is an another advantages for our proposed OMT map.

4.3. **2P-Crop-OMT-UNetB algorithm for Sub-Sahara-Africa Adult Glioma and Intracranial Meningioma Challenge.** To reduce the spending time of computing OMT tensors in Phase I-OMT for the inference, we use 2P-Crop-OMT-UNetB algorithm with SegResNet to predict and segment the tumor regions of Sub-Sahara-Africa Adult Glioma and Intracranial Meningioma Challenge. The OMT tensors of the validation samples in Phase II are constructed by using $\gamma = 1.5$. The Dice scores of WT, TC, and ET are listed in Table 5. The statistical analysis of the Dice scores is shown in Figure 8.

TABLE 5. Dice score of the online validation by using 2P-Crop-OMT-UNetB with SegResNet

	Sub-Sahara-Africa			Intracranial Meningioma		
	WT	TC	ET	WT	TC	ET
mean	0.8747	0.8344	0.8267	0.8316	0.8395	0.8401
sd	0.1347	0.2507	0.2343	0.2725	0.2782	0.2799
25 quantile	0.8624	0.8862	0.8628	0.8838	0.8778	0.8923
median	0.9206	0.9219	0.9091	0.9440	0.9581	0.9594
75 quantile	0.9369	0.9480	0.9192	0.9655	0.9793	0.9779

There are 1, 3, and 2 outliers of WT, TC, and ET, respectively, for the sub-Sahara-Africa adult glioma as shown in Figure 8a. The Dice scores of these outliers are obviously less than that of the other samples. Except these outliers, we can get high Dice scores of WT, TC, and ET for 25 quantile, median, and 75 quantile even the training data of sub-Sahara-Africa adult glioma has only 48 samples.

There are 23, 22, and 23 outliers of WT, TC, and ET, respectively, in the 141 online validation samples for the intracranial meningioma. The Dice scores of WT, TC, and ET for these outliers are less than 0.7480, 0.6797, and 0.7535, respectively. The results in Table 5 show that 2P-Crop-OMT-UNetB with SegResNet can get very well predictions of WT, TC, and ET for the 25 quantile, median, and 75 quantile of the Dice scores.

5. DISCUSSION

In this paper, we propose an UNet-based brain tumor segmentation framework via OMT-based preprocessing. The OMT map transforms an irregular domain to a solid unit ball with minimal deformation and keeping the global information of the original image. Through the density control, it can enlarge the tumor proportion to help the detection and segmentation of the model. Moreover, data augmentation by using different density parameters can increase the data diversity to enhance the model generalization ability.

Two phase processes with OMT maps are used to detect and segment the tumor region of Tasks 1 (adult glioma), 2 (BraTS-Africa adult glioma) and 3 (meningioma) in Brain Tumor Segmentation 2023 Cluster of Challenges. In Phase I, UNet-based model with OMT tensors or random crop tensors as the input tensors to predict the possible WT region of validation and testing data and then expand the 4 pixels by morphology dilation as the domain of the density function in Phase II. The OMT tensors with the new densities are re-constructed to train and inference the data in Tasks 1, 2, and 3.

By using SegResNet training model, the Dices scores of (WT, TC, ET) of the online validations are (0.9214, 0.8823, 0.8411), (0.8747, 0.8344, 0.8267), and (0.8316, 0.8395, 0.8401) for Tasks 1, 2, and 3, respectively. We have very well predictions of WT, TC, and ET for Task 1. The 25 quantile of the Dice scores

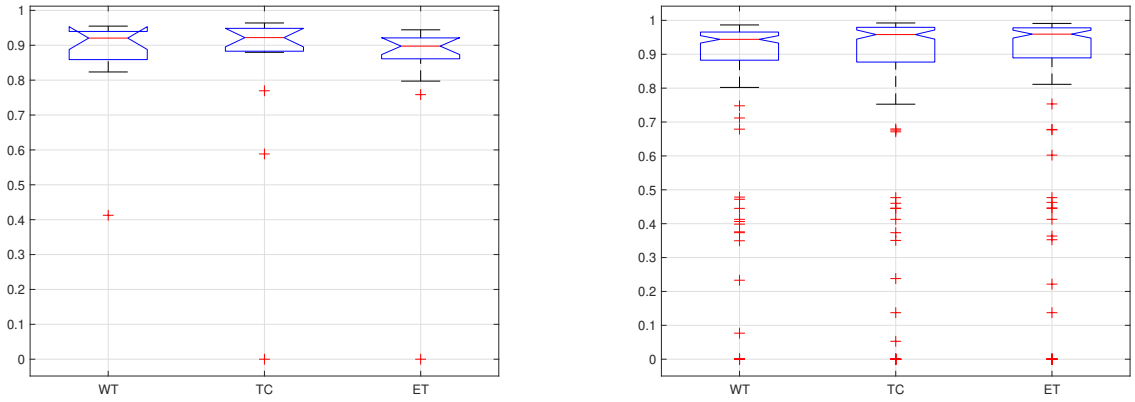

(A) sub-Sahara-Africa adult glioma

(B) intracranial meningioma

FIGURE 8. Statistical analysis for Dice scores of online validation data for sub-Sahara-Africa adult glioma and intracranial meningioma

of (WT, TC, ET) for Tasks 2 and 3 are (0.8624, 0.8862, 0.8628) and (0.8838, 0.8778, 0.8923), which are well predictions. These results demonstrate that our proposed 2-phase UNet-based machine learning with OMT pre-processing is suitable for the segmentation of different types of brain tumors.

Some of the brain images and the associated tumor regions for the cross-validation are shown in Figure 9. We can see that the tumor regions are dark. Due to the smaller density function value in the dark gray area, its proportion in the OMT tensors is also smaller than in the original image. This leads to less accurate predictions of this area. The choice of a more effective density function to improve the prediction accuracy of the dark gray regions is one of our main research topics in the near future.

STATEMENTS AND DECLARATIONS

The authors declare that they have no conflict of interest, and the manuscript has no associated data.

ACKNOWLEDGMENTS

This work was partially supported by the National Science and Technology Council (NSTC) and the National Center for Theoretical Sciences. T.-M. Huang and W.-W. Lin were partially supported by NSTC 110-2115-M-003-012-MY3 and NSTC 112-2115-M-A49-010-, respectively.

REFERENCES

[1] U. Baid, S. Ghodasara, M. Bilello, S. Mohan, E. Calabrese, E. Colak, K. Farahani, J. Kalpathy-Cramer, F. C. Kitamura, S. Pati, L. M. Prevedello, J. D. Rudie, C. Sako, R. T. Shinohara, T. Bergquist, R. Chai, J. Eddy, J. Elliott, W. Reade, T. Schaffter, T. Yu, J. Zheng, B. Annotators, C. Davatzikos, J. Mongan, C. Hess, S. Cha, J. Villanueva-Meyer, J. B. Freymann, J. S. Kirby, B. Wiestler, P. Crivellaro, R. R. Colen, A. Kotrotsou, D. Marcus, M. Milchenko, A. Nazeri, H. Fathallah-Shaykh, R. Wiest, A. Jakab, M.-A. Weber, A. Mahajan, B. Menze, A. E. Flanders, and S. Bakas. The RSNA-ASNR-MICCAI BraTS 2021 benchmark on brain tumor segmentation and radiogenomic classification. Preprint at https://arxiv.org/abs/2107.02314, 2021.

[2] S. Bakas, H. Akbari, A. Sotiras, M. Bilello, M. Rozycki, J. Kirby, J. Freymann, K. Farahani, and C. Davatzikos. Segmentation labels and radiomic features for the pre-operative scans of the TCGA-GBM collection. The Cancer Imaging Archive, DOI:10.7937/K9/TCIA.2017.KLXWJJ1Q, 2017.

[3] S. Bakas, H. Akbari, A. Sotiras, M. Bilello, M. Rozycki, J. Kirby, J. Freymann, K. Farahani, and C. Davatzikos. Segmentation labels and radiomic features for the pre-operative scans of the TCGA-LGG collection. The Cancer Imaging Archive, DOI:10.7937/K9/TCIA.2017.GJQ7R0EF, 2017.

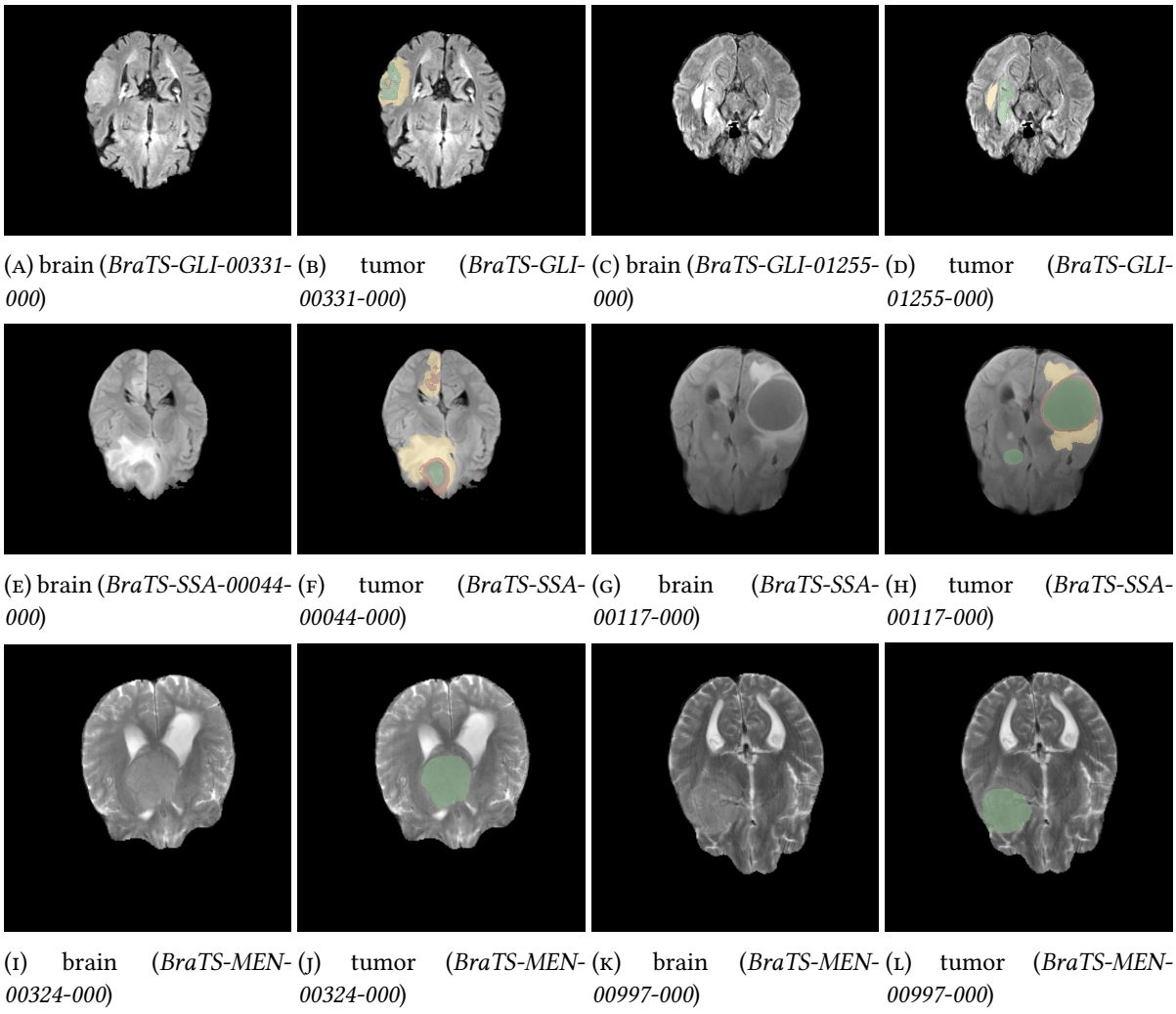

(A) brain (*BraTS-GLI-00331-000*) (B) tumor (*BraTS-GLI-00331-000*) (C) brain (*BraTS-GLI-01255-000*) (D) tumor (*BraTS-GLI-01255-000*)

(E) brain (*BraTS-SSA-00044-000*) (F) tumor (*BraTS-SSA-00044-000*) (G) brain (*BraTS-SSA-00117-000*) (H) tumor (*BraTS-SSA-00117-000*)

(I) brain (*BraTS-MEN-00324-000*) (J) tumor (*BraTS-MEN-00324-000*) (K) brain (*BraTS-MEN-00997-000*) (L) tumor (*BraTS-MEN-00997-000*)

FIGURE 9. 2D brain images and the associated tumor regions. (a)-(d) Task 1: adult glioma, (e)-(h) Task 2: BraTS-Africa, (i)-(l) Task 3: meningioma

[4] S. Bakas, H. Akbari, A. Sotiras, M. Bilello, M. Rozycki, J. S. Kirby, J. B. Freymann, K. Farahani, and C. Davatzikos. Advancing the cancer genome atlas glioma MRI collections with expert segmentation labels and radiomic features. *Sci. Data*, 4:170117, 2017.

[5] P. Chao, C.-Y. Kao, Y. Ruan, C.-H. Huang, and Y.-L. Lin. HarDNet: A low memory traffic network. In *2019 IEEE/CVF International Conference on Computer Vision (ICCV)*, pages 3552–3561, 2019.

[6] Y. Choi, S. Bae, J. Chang, S.-G. Kang, S. Kim, J. Kim, T. Rim, S. Choi, R. Jain, and S.-K. Lee. Fully automated hybrid approach to predict the IDH mutation status of gliomas via deep learning and radiomics. *Neuro-Oncology*, 23(2):304–313, 2021.

[7] Ö. Çiçek, A. Abdulkadir, S. S. Lienkamp, T. Brox, and O. Ronneberger. 3D U-Net: Learning dense volumetric segmentation from sparse annotation. In *Medical Image Computing and Computer-Assisted Intervention – MICCAI 2016*, pages 424–432, 2016.

[8] J. Cluceru, Y. Interian, J. J. Phillips, A. M. Molinaro, T. L. Luks, P. Alcaide-Leon, M. P. Olson, D. Nair, M. LaFontaine, A. Shai, P. Chunduru, V. Pedoia, J. E. Villanueva-Meyer, S. M. Chang, and J. M. Lupo. Improving the noninvasive classification of glioma genetic subtype with deep learning and diffusion-weighted imaging. *Neuro-Oncology*, 24(4):639–652, 2022.

[9] D. C. Gutman and R. J. Young. IDH glioma radiogenomics in the era of deep learning. *Neuro-Oncology*, 23(2):182–183, 2021.

[10] A. Hatamizadeh, V. Nath, Y. Tang, D. Yang, H. Roth, and D. Xu. Swin UNETR: Swin transformers for semantic segmentation of brain tumors in MRI images. In *International MICCAI Brainlesion Workshop*, pages 272–284, 2021.

[11] T.-M. Huang, W.-H. Liao, W.-W. Lin, M.-H. Yueh, and S.-T. Yau. Convergence analysis of volumetric stretch energy minimization and its associated optimal mass transport. *SIAM Journal on Imaging Sciences*, 16(3):1825–1855, 2023.

[12] T.-M. Huang, W.-H. Liao, and W.-W. L. Lin. Fundamental theory and R-linear convergence of stretch energy minimization for spherical equiareal parameterization. *Journal of Numerical Mathematics*, 32:1–25, 2024.

[13] F. Isensee, P. Jaeger, S. Kohl, J. Petersen, and K. Maier-Hein. nnU-Net: a self-configuring method for deep learning-based biomedical image segmentation. *Nature Methods*, 18:203–211, 2021.

[14] W.-W. Lin, C. Juang, M.-H. Yueh, T.-M. Huang, T. Li, S. Wang, and S.-T. Yau. 3D brain tumor segmentation using a two-stage optimal mass transport algorithm. *Scientific Reports*, 11:14686, 2021.

[15] W.-W. Lin, J.-W. Lin, T.-M. Huang, T. Li, M.-H. Yueh, and S.-T. Yau. A novel 2-phase residual U-net algorithm combined with optimal mass transportation for 3D brain tumor detection and segmentation. *Scientific Reports*, 12(1):6452, 2022.

[16] J. Long, E. Shelhamer, and T. Darrell. Fully convolutional networks for semantic segmentation. In *Proceedings of the IEEE conference on computer vision and pattern recognition*, pages 3431–3440, 2015.

[17] H. M. Luu and S.-H. Park. Extending nn-UNet for brain tumor segmentation. In *International MICCAI Brainlesion Workshop*, pages 173–186. Springer, 2021.

[18] R. McKinley, R. Meier, and R. Wiest. Ensembles of densely-connected CNNs with label-uncertainty for brain tumor segmentation. In *Brainlesion: Glioma, Multiple Sclerosis, Stroke and Traumatic Brain Injuries*, pages 456–465, 2018.

[19] B. H. Menze, A. Jakab, S. Bauer, J. Kalpathy-Cramer, K. Farahani, J. Kirby, Y. Burren, N. Porz, J. Slotboom, R. Wiest, L. Lanczi, E. Gerstner, M. Weber, T. Arbel, B. B. Avants, N. Ayache, P. Buendia, D. L. Collins, N. Cordier, J. J. Corso, A. Criminisi, T. Das, H. Delingette, ç. Demiralp, C. R. Durst, M. Dojat, S. Doyle, J. Festa, F. Forbes, E. Geremia, B. Glocker, P. Golland, X. Guo, A. Hamamci, K. M. Iftekharuddin, R. Jena, N. M. John, E. Konukoglu, D. Lashkari, J. A. Mariz, R. Meier, S. Pereira, D. Precup, S. J. Price, T. R. Raviv, S. M. S. Reza, M. Ryan, D. Sarikaya, L. Schwartz, H. Shin, J. Shotton, C. A. Silva, N. Sousa, N. K. Subbanna, G. Szekely, T. J. Taylor, O. M. Thomas, N. J. Tustison, G. Unal, F. Vasseur, M. Wintermark, D. H. Ye, L. Zhao, B. Zhao, D. Zikic, M. Prastawa, M. Reyes, and K. Van Leemput. The multimodal brain tumor image segmentation benchmark (BRATS). *IEEE Transactions on Medical Imaging*, 34(10):1993–2024, 2014.

[20] A. Myronenko. 3D MRI brain tumor segmentation using autoencoder regularization. In *International MICCAI Brainlesion Workshop*, pages 311–320. Springer, 2019.

[21] G. Reifenberger, H.-G. Wirsching, C. B. Knobbe-Thomsen, and M. Weller. Advances in the molecular genetics of gliomas - implications for classification and therapy. *Nature Reviews Clinical Oncology*, 14:434–452, 2017.

[22] O. Ronneberger, P. Fischer, and T. Brox. U-net: Convolutional networks for biomedical image segmentation. In *Lecture Notes in Computer Science*, pages 234–241. 2015.

[23] The MONAI Consortium. Project MONAI, Dec 2020.

[24] J. Wu, Q. Xu, Y. Shen, W. Chen, K. Xu, and X.-R. Qi. Swin transformer improves the IDH mutation status prediction of gliomas free of MRI-based tumor segmentation. *Journal of Clinical Medicine*, 11(15):4625, 2022.

[25] X. Xiao, S. Lian, Z. Luo, and S. Li. Weighted Res-UNet for high-quality retina vessel segmentation. In *2018 9th International Conference on Information Technology in Medicine and Education (ITME)*, pages 327–331, 2018.

[26] M.-H. Yueh, T.-M. Huang, T. Li, W.-W. Lin, and S.-T. Yau. Projected gradient method combined with homotopy techniques for volume-measure-preserving optimal mass transportation problems. *Journal of Scientific Computing*, 88(64):1–24, 2021.

[27] M.-H. Yueh, T. Li, W.-W. Lin, and S.-T. Yau. A novel algorithm for volume-preserving parameterizations of 3-manifolds. *SIAM Journal on Imaging Sciences*, 12(2):1071–1098, 2019.

[28] M.-H. Yueh, W.-W. Lin, C.-T. Wu, and S.-T. Yau. A novel stretch energy minimization algorithm for equiareal parameterizations. *Journal of Scientific Computing*, 78(3):1353–1386, 2019.

[29] R. Zeineldin, M. Karar, O. Burgert, and F. Mathis-Ullrich. Multimodal CNN networks for brain tumor segmentation in MRI: A BraTS 2022 challenge solution. In *Brainlesion: Glioma, Multiple Sclerosis, Stroke and Traumatic Brain Injuries*, pages 127–137, 2023.

[30] R. Zeineldin, M. Karar, J. Coburger, C. Wirtz, and O. Burgert. DeepSeg: deep neural network framework for automatic brain tumor segmentation using magnetic resonance FLAIR images. *International Journal of Computer Assisted Radiology and Surgery*, 15:909–920, 2020.